Topological superfluid of *s*-wave-interacting fermions by engineered orbital hybridization in an optical lattice

Maksims Arzamasovs,[1] Shuai Li,[1] Shuqi Han,[1] W. Vincent Liu,[2,3,*] and Bo Liu[1,†]

[1]*Ministry of Education Key Laboratory for Nonequilibrium Synthesis and Modulation of Condensed Matter, Shaanxi Province Key Laboratory of Quantum Information and Quantum Optoelectronic Devices, School of Physics, Xi'an Jiaotong University, Xi'an 710049, China*

[2]*Department of Physics and Astronomy, University of Pittsburgh, Pittsburgh, Pennsylvania 15260, USA*

[3]*Department of Physics and Shenzhen Institute for Quantum Science and Engineering, Southern University of Science and Technology, Shenzhen, 518055, China*

(Received 17 January 2021; revised 8 September 2022; accepted 23 February 2023; published 10 March 2023)

Recent advanced experimental implementations of optical lattices with highly tunable geometry open up new regimes for exploring quantum many-body states of matter that had not been accessible previously. Here we report that a topological fermionic superfluid with higher Chern number emerges spontaneously from *s*-wave spin-singlet pairing in an orbital optical lattice when its geometry is tuned to explicitly break reflection symmetry. Qualitatively distinct from the conventional scheme that relies on higher partial-wave pairing, the crucial ingredient of our model is topology originating from mixing higher Wannier orbitals. It leads to unexpected changes in the topological band structure at the single-particle level, i.e., the bands are transformed from possessing two flux-π Dirac points into a single quadratic touching point with flux 2π. Based on such engineered single-particle bands, spin-singlet pairing of ultracold fermions arising from standard *s*-wave attractive interaction is found to induce higher Chern number (Chern number of 2) and topologically protected chiral edge modes, all occurring at a higher critical temperatures in relative scales, potentially circumventing one of the major obstacle for its realization in ultracold gases.

DOI: 10.1103/PhysRevA.107.033309

I. INTRODUCTION

Pursuit of topological phases of matter has been one of the central thrusts in condensed-matter physics since the discovery of the chiral-*A* phase of superfluid ^{3}He [1] and quantum Hall effect [2–5]. The concept of topology not only plays a key role in a variety of exotic quantum phenomena, such as topological insulators, chiral superconductors, and Weyl semimetals, but also is closely related to fundamental physics, e.g., it allows to distinguish new phases of matter that cannot be described by Landau's theory of symmetry breaking [6,7]. It has, thus, explosively triggered a tremendous amount of effort in both theoretical and experimental studies in solids. Besides that, there has been a great interest in simulating topological matter with ultracold gases. Such highly controllable platforms not only provide versatile tools for simulating electronic systems, but also present possibilities for studying new phenomena with no counterparts in solids. Recent experimental advances in ultracold gases, such as creating tunable spin-orbit coupling [8–16] and simulating Aharonov-Bohm and quantum anomalous Hall effects [17–20], provide unprecedented opportunities for finding topological states of matter. Moreover, hybridization of higher orbital bands has opened a completely different avenue for emulating spin-orbit coupling, or artificial gauge fields, in general, in ultracold atoms [21–27], yielding various interesting quantum states of matter [28–34].

In this paper, we report a mechanism of constructing higher Chern number superfluidity by engineered single-particle band structure through spin-singlet pairing by the standard *s*-wave attraction. The key idea here is to utilize a symmetry-based method to systematically control the non-trivial hybridization between higher orbitals of ultracold atoms in optical lattices. Surprisingly, we find that such an orbital mixing leads to unexpected changes in the topological band structure at the single-particle level. When further considering *s*-wave attraction between fermionic atoms, a spin-singlet pairing induced higher Chern number superfluid emerges in the presence of on-site rotation. This idea is motivated by recent experimental progresses in manipulating higher orbital bands in optical lattices, such as the breakthrough observation of long-lived *p*-band ultracold atoms [24–27,35,36]. It opens up a new thrust towards investigating exotic many-body phases with orbital degrees of freedom [29,30,32–34,37–44]. As we will show below, symmetry-based manipulations of nontrivial orbital hybridization can lead to other undiscovered results.

II. ORBITAL-HYBRIDIZED TOPOLOGICAL BANDS

Let us consider a gas of ultracold fermions, loaded into a two-dimensional (2D) optical lattice realized from a strongly anisotropic three-dimensional lattice. Specifically, the lattice potential is expressed as $V_{\mathrm{OL}}(\mathbf{r}) = -V_x \cos^2(k_{Lx}x) -$

*wvliu@pitt.edu
†liubophy@gmail.com

$V_y \cos^2(k_{Ly}y) - V_z \cos^2(k_{Lz}z)$ with k_{Lx}, k_{Ly}, and k_{Lz} being the wave vectors of respective laser fields. The corresponding lattice constants are $a_x = \pi/k_{Lx}$, $a_y = \pi/k_{Ly}$, and $a_z = \pi/k_{Lz}$. We focus on the case with $V_z \gg V_x, V_y$ and the system behaves dynamically as a 2D system. In the deep lattice limit, lattice potentials at each site can be approximated as harmonic oscillators. Under this approximation, the requirement of $V_x k_{Lx}^2 = V_y k_{Ly}^2 = V_z k_{Lz}^2$ preserves the local SO(3) rotation symmetry, which guarantees threefold degeneracy of the p orbitals locally. When further adjusting lattice depth or lattice spacing, parameters of the potential can be tuned as $\alpha V_x k_{Lx}^2 = V_y k_{Ly}^2 = V_z k_{Lz}^2$. When $\alpha \neq 1$, a finite orbital Zeeman splitting between p_x and p_y (p_z) orbitals can be introduced [37]. The key ingredient here is the breaking of z-directional inversion symmetry, which can induce nontrivial hybridization between p_x (p_y) and p_z orbitals, respectively, which could be achieved through designing optical lattices with nonstandard geometry. For instance, we can consider including a magnetic-field gradient [19,20], or an additional standing wave pattern along the z direction. The corresponding single-particle Hamiltonian can, thus, be expressed as either $H_0 = -\frac{\hbar^2}{2m}\nabla^2 + V_{\rm OL}(\mathbf{r}) - \mathbf{F}\cdot\mathbf{r}$ with the force $\mathbf{F} = -J\,\nabla_z B$ applied to the atom with spin magnetic moment J, or $H_0 = -\frac{\hbar^2}{2m}\nabla^2 + V_{\rm OL}(\mathbf{r}) + V_{\bar{z}}\cos^2(3k_{Lz}z + \theta/2)$, with the lattice depth $V_{\bar{z}}$ and $\theta \neq \pi$ [$\theta \in (0, 2\pi)$], respectively. The p-orbital fermions can, thus, be described by the following multiorbital model in the tight-binding regime,

$$
\begin{aligned}
\mathbf{H}_0 =& t_\parallel \sum_{\mathbf{r_i}} C^\dagger_{p_x}(\mathbf{r_i}) C_{p_x}(\mathbf{r_i} + \vec{e}_x) - t_\perp \sum_{\mathbf{r_i}} C^\dagger_{p_x}(\mathbf{r_i}) C_{p_x}(\mathbf{r_i} + \vec{e}_y) \\
&+ t'_\parallel \sum_{\mathbf{r_i}} C^\dagger_{p_y}(\mathbf{r_i}) C_{p_y}(\mathbf{r_i} + \vec{e}_y) \\
&- t'_\perp \sum_{\mathbf{r_i}} C^\dagger_{p_y}(\mathbf{r_i}) C_{p_y}(\mathbf{r_i} + \vec{e}_x) - t_z \sum_{\mathbf{r_i}} C^\dagger_{p_z}(\mathbf{r_i}) C_{p_z}(\mathbf{r_i} + \vec{e}_x) \\
&- t'_z \sum_{\mathbf{r_i}} C^\dagger_{p_z}(\mathbf{r_i}) C_{p_z}(\mathbf{r_i} + \vec{e}_y) \\
&+ t_m \sum_{\mathbf{r_i}} \left[C^\dagger_{p_x}(\mathbf{r_i} + \vec{e}_x) C_{p_z}(\mathbf{r_i}) - C^\dagger_{p_x}(\mathbf{r_i}) C_{p_z}(\mathbf{r_i} + \vec{e}_x) \right] \\
&+ t'_m \sum_{\mathbf{r_i}} \left[C^\dagger_{p_y}(\mathbf{r_i} + \vec{e}_y) C_{p_z}(\mathbf{r_i}) - C^\dagger_{p_y}(\mathbf{r_i}) C_{p_z}(\mathbf{r_i} + \vec{e}_y) \right] \\
&+ \text{H.c.} - \delta\mu_x \sum_{\mathbf{r_i}} C^\dagger_{p_x}(\mathbf{r_i}) C_{p_x}(\mathbf{r_i}), \qquad (1)
\end{aligned}
$$

where $C^\dagger_\nu(\mathbf{r_i})$ and $C_\nu(\mathbf{r_i})$ with $\nu = p_x, p_y, p_z$ are fermionic creation and annihilation operators for particles occupying orbitals ν at lattice sites $\mathbf{r_i}$. $t_\parallel(t'_\parallel)$ and $t_\perp(t'_\perp)$ are longitudinal and transverse hopping amplitudes, respectively. Relative signs of the amplitudes are fixed by parities of p_x and p_y orbitals. $t_z(t'_z)$ describes hopping of p_z fermions on the xy plane. The key ingredient here is hybridization among p_x and p_z, p_y, and p_z orbitals, characterized by t_m and t'_m in Eq. (1). Such hybridization arises from the asymmetric shape of p_z orbital wave functions induced by inversion symmetry breaking in the z direction, which is highly tunable through varying magnetic-field gradient $\nabla_z B$ or lattice depth $V_{\bar{z}}$, as shown in Fig. 5 of the Appendix. $\delta\mu_x \sum_{\mathbf{r_i}} C^\dagger_{p_x}(\mathbf{r_i}) C_{p_x}(\mathbf{r_i})$ is the orbital Zeeman splitting term. In the momentum space, Eq. (1) can be rewritten as

$$
\mathbf{H}_0(\mathbf{k}) = [C^\dagger_{p_x}(\mathbf{k}) C^\dagger_{p_y}(\mathbf{k}) C^\dagger_{p_z}(\mathbf{k})]\,\mathscr{H}(\mathbf{k}) \begin{pmatrix} C_{p_x}(\mathbf{k}) \\ C_{p_y}(\mathbf{k}) \\ C_{p_z}(\mathbf{k}) \end{pmatrix},
$$

where

$$
\mathscr{H}(\mathbf{k}) = \begin{pmatrix} 2t_\parallel \cos(k_x a_x) - 2t_\perp \cos(k_y a_y) - \delta\mu_x & 0 & 2it_m \sin(k_x a_x) \\ 0 & 2t'_\parallel \cos(k_y a_y) - 2t'_\perp \cos(k_x a_x) & 2it'_m \sin(k_y a_y) \\ -2it_m \sin(k_x a_x) & -2it'_m \sin(k_y a_y) & -2t_z \cos(k_x a_x) - 2t'_z \cos(k_y a_y) \end{pmatrix}, \qquad (2)
$$

with lattice momentum $\mathbf{k} = (k_x, k_y)$ taking values in the first Brillouin zone, and $C^\dagger_\nu(\mathbf{k})$ and $C_\nu(\mathbf{k})$ representing ν-orbital fermionic creation and annihilation operators in momentum space. Eigenvalues of Eq. (2) result in the single-particle band structure. Qualitatively distinct from previous studies where the D_4 point-group symmetry was a necessary requirement [28,45], our model generalizes to the case where such a point-group symmetry can be turned on or off. In the presence of finite orbital Zeeman splitting, the D_4 symmetry is explicitly broken. Consequently, two Dirac band touching points appear between the second and the third bands [Fig. 1(a)], which are protected by a reflection symmetry associated with the following transformations of the fermionic operators: $\mathcal{R}_\parallel \equiv \{C_{p_x}(\mathbf{r_i}) \to -C_{p_x}(-\mathbf{r}_{ix}, \mathbf{r}_{iy}), C_{p_{y(z)}}(\mathbf{r_i}) \to C_{p_{y(z)}}(-\mathbf{r}_{ix}, \mathbf{r}_{iy})\}$ and $\mathcal{R}_\perp \equiv \{C_{p_{x(z)}}(\mathbf{r_i}) \to C_{p_{x(z)}}(\mathbf{r}_{ix}, -\mathbf{r}_{iy}),\ C_{p_y}(\mathbf{r_i}) \to -C_{p_y}(\mathbf{r}_{ix}, -\mathbf{r}_{iy})\}$. When the orbital Zeeman term vanishes, $\delta\mu_x = 0$, and the D_4 symmetry is restored, the two Dirac touching points are found to merge together and form a quadratic band touching at $\Gamma(k_x = 0, k_y = 0)$ [Fig. 1(c)]. Therefore, from the symmetry point of view, our model is substantially different from previous works [28,45], which can be considered special, higher-symmetry cases of our model. Single-particle topology further shows new features associated with the above variation of the band structure. When $\delta\mu_x \neq 0$, the effective Hamiltonian near one of the Dirac touching points $(k_{\rm Dirac}, 0)$ can be expressed as

$$
\mathbf{H}^{\rm Dirac}_{\rm eff} = c'_0 k'_x \mathbb{I}_{2\times 2} + c'_1 k_y \sigma_x + c'_3 k'_x \sigma_z, \qquad (3)
$$

where $k'_x = k_x - k_{\rm Dirac}$, expressions for c'_0, c'_1, and c'_3 are quoted in Appendix A, and ($\mathbb{I}_{2\times 2}$, σ_x, σ_z) are the unit and Pauli matrices. As shown in Fig. 1(b), a 2D vector field $\mathbf{h}^{\rm Dirac}(\mathbf{k}) = (c'_3 k'_x, c'_1 k_y)$ surrounding the Dirac touching point forms a vortex structure with winding number 1, characterizing its topological nontriviality. When $\delta\mu_x = 0$, it turns out that the quadratic touching point forms a topological defect

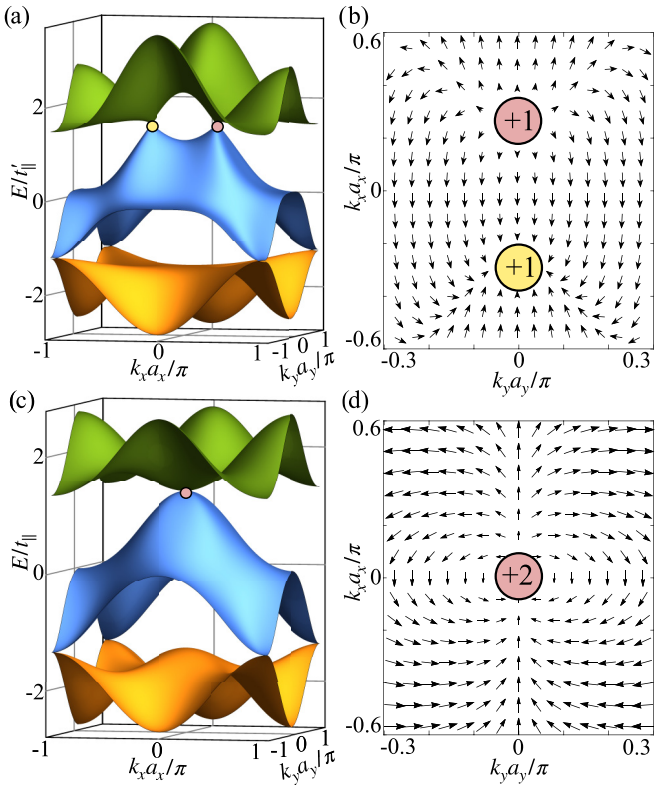

FIG. 1. (a) and (c): Single-particle energy spectra of the tight-binding model in Eq. (1) for $\delta\mu_x = 0.5t'_\parallel$ and $\delta\mu_x = 0$, respectively. (b) and (d): The topological defects formed around Dirac and quadratic band touching points, respectively. In (a), other parameters are chosen as $t_\parallel/t'_\parallel = 1.2$, $t_\perp = t'_z = 0.3t'_\parallel$, $t'_\perp/t_\perp = 1.2$, $t'_m/t_m = 0.8$, $t_z/t'_z = 1.2$, and $t_m = 0.6t'_\parallel$. In (c), we choose $t_\parallel/t'_\parallel = t_\perp/t'_\perp = t_m/t'_m = t_z/t'_z = 1$, $t_m = 0.6t_\parallel$ and $t_z = t_\perp = 0.3t_\parallel$.

with winding number 2 (see details in Appendix A), such as shown in Fig. 1(d). Therefore, in our model the topological defect in the single-particle spectrum can be transferred from two Dirac points to the single quadratic touching point. Topological properties of the two cases are closely linked since the winding number for the quadratic touching is exactly the sum of those for the two Dirac points. This effect found here makes our proposal topologically distinguishable from the previous studies [28,45].

III. s-WAVE INTERACTION INDUCED HIGHER CHERN NUMBER SUPERFLUID

The next intriguing question is whether interactions can destabilize topological bands discussed above and lead to novel many-body phases. For instance, past studies have shown that quadratic touching is unstable under repulsion, resulting in topological insulators and nematic phases [28,46–49]. However, when considering contact attraction, spin-singlet superconducting pairing is absent since it is marginally irrelevant in the renormalization-group analysis [49]. In the following, we are going to show that, unexpectedly, in the presence of on-site rotation a higher Chern number superfluid can be created by the s-wave attraction-induced spin-singlet pairing. To that end, consider loading attractive spin-1/2 fermionic atoms into the lattice system described above. With the addition of on-site rotation, the interacting model can be expressed as

$$\mathbf{H} = \mathbf{H}_{0,\sigma} + \mathbf{H}_{\rm int} + \mathbf{H}_L. \tag{4}$$

The interaction part $\mathbf{H}_{\rm int}$ is

$$\begin{aligned}\mathbf{H}_{\rm int} = \sum_{\mathbf{r_i}} \Big\{ & U \sum_{\nu} n(\mathbf{r_i})_{\nu,\uparrow} n(\mathbf{r_i})_{\nu,\downarrow} + W \sum_{\nu\neq\rho} [n(\mathbf{r_i})_{\nu,\uparrow} n(\mathbf{r_i})_{\rho,\downarrow} \\ & + C^\dagger_{\nu,\uparrow}(\mathbf{r_i}) C^\dagger_{\rho,\downarrow}(\mathbf{r_i}) C_{\nu,\downarrow}(\mathbf{r_i}) C_{\rho,\uparrow}(\mathbf{r_i}) \\ & + C^\dagger_{\nu,\uparrow}(\mathbf{r_i}) C^\dagger_{\nu,\downarrow}(\mathbf{r_i}) C_{\rho,\downarrow}(\mathbf{r_i}) C_{\rho,\uparrow}(\mathbf{r_i})] \Big\}, \end{aligned} \tag{5}$$

where $n_{\nu,\sigma}(\mathbf{r_i}) \equiv C^\dagger_{\nu,\sigma}(\mathbf{r_i}) C_{\nu,\sigma}(\mathbf{r_i})$ is the density operator.

The intraorbital and interorbital interaction strengths are captured by U and W, respectively. Since here we consider employing an additional standing wave to break the z-directional inversion symmetry, fermions of both spins are experiencing the same lattice potentials. Therefore, noninteracting Hamiltonian $\mathbf{H}_{0,\sigma}$ does not depend on spin. $\mathbf{H}_L = i\Omega_z \sum_{\mathbf{r_i},\sigma} [C^\dagger_{p_x,\sigma}(\mathbf{r_i}) C_{p_y,\sigma}(\mathbf{r_i}) - C^\dagger_{p_y,\sigma}(\mathbf{r_i}) C_{p_x,\sigma}(\mathbf{r_i})]$ describes the on-site rotation, which has been achieved in a triangular lattice [50,51]. Through utilizing electro-optic phase modulation of the laser beams, we propose a method to realize the on-site rotation in our setup (see Appendix B for details). Attractive fermions tend to pair with each other and form a superfluid at low temperatures. To study it, we construct a path-integral formalism. Details are given in Appendix C. Under the saddle-point approximation, surprisingly, we find that by simply tuning the average filling n of fermions, superfluids with distinct topological properties can be achieved. The Bogoliubov–de Gennes (BdG) Hamiltonian (given in Appendix C) describing this superfluid preserves the particle-hole symmetry, i.e., $\Xi H_{\rm BdG}(\mathbf{k})\Xi^{-1} = -H^*_{\rm BdG}(-\mathbf{k})$ with $\Xi \equiv \left(\begin{smallmatrix} 0 & \mathbb{I}_{3\times3} \\ \mathbb{I}_{3\times3} & 0 \end{smallmatrix}\right) \otimes \sigma_y$, whereas the time-reversal and chiral symmetries are broken. Therefore, it belongs to D symmetry class of the tenfold classification [52], and topology of the superfluid can, thus, be evaluated by the Chern number,

$$C = \frac{1}{2\pi} \sum_n \int \Omega^n(k_x, k_y) dk_x dk_y, \tag{6}$$

where summation of n runs over all the occupied bands of $H_{\rm BdG}$.

$$\begin{aligned}&\Omega^n(k_x, k_y) \\ &= i \sum_{n'\neq n} \left[\frac{\langle n|\partial_{k_x} H_{\rm BdG}|n'\rangle \langle n'|\partial_{k_y} H_{\rm BdG}|n\rangle}{(E_n - E_{n'})^2} - (k_x \leftrightarrow k_y) \right] \end{aligned} \tag{7}$$

is the Berry curvature and $|n(n')\rangle$ stand for the eigenstate with energies $E_{n(n')}$. Figure 2 shows the topological phase diagram. Interestingly, it is shown that both for case $\delta\mu_x \neq 0$ (Dirac touching) as well as $\delta\mu_x = 0$ (quadratic touching) topological phase diagrams are qualitatively similar. There are two different topological regimes characterized by distinct Chern numbers. Intriguingly, a new topological orbital-hybridized superfluid with higher Chern number ($C = 2$) is unveiled. For fixed interaction strength, the system undergoes a topological

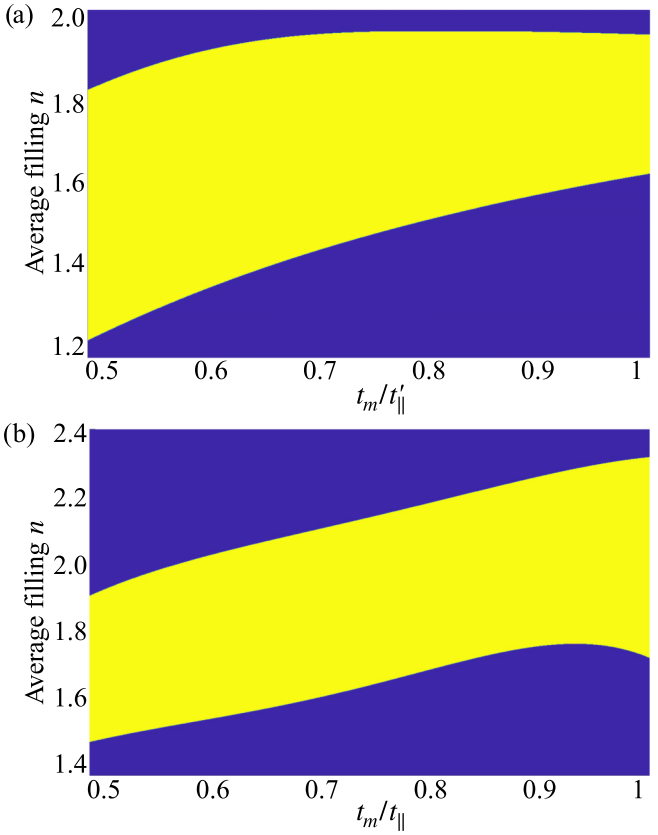

FIG. 2. (a) and (b) Topological phase diagram as a function of orbital mixing strength and the average filling for $\delta\mu_x = 0.5t'_\parallel$ and $\delta\mu_x = 0$, respectively. The topologically nontrivial (yellow area) and trivial (purple area) superfluids are separated, and the phase boundary corresponds to the closing of the bulk gap. In (a) we choose $|W| = 0.5t'_\parallel$, $U = 3W$, $\Omega_z = 0.5t'_\parallel$ and other parameters are the same as in Fig. 1(a). In (b) we choose $|W| = 0.5t_\parallel$, $U = 3W$, $\Omega_z = 0.5t_\parallel$ and other parameters are the same as in Fig. 1(c).

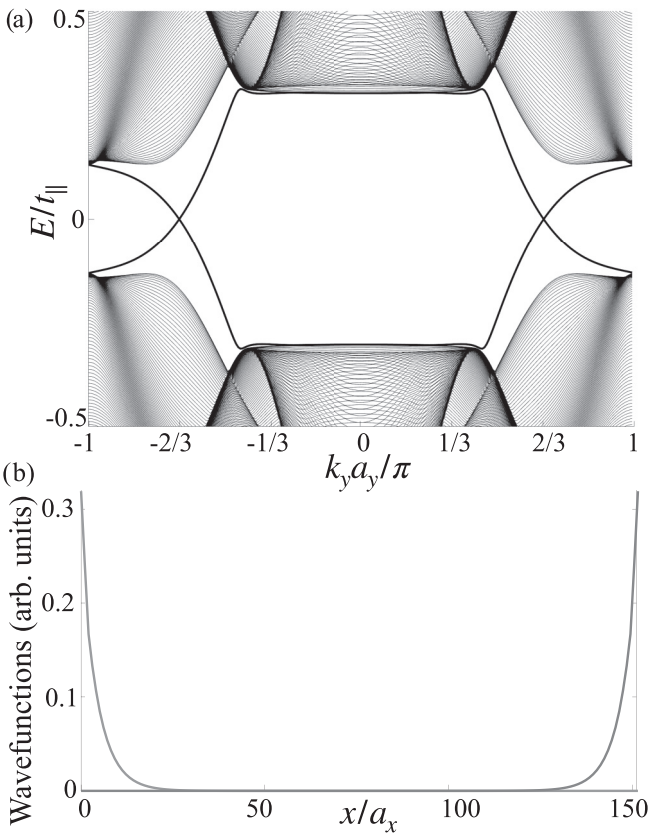

FIG. 3. (a) Energy spectrum of the tSF state under the open (periodic) boundary condition in the $x(y)$ direction. The in-gap modes are two pairs of chiral edge states. (b) The amplitudes of wave functions for the two chiral edge modes with $k_y a_y = 2\pi/3$ in (a). Here we choose $t_m = 0.8t_\parallel$ and $n = 1.6$. Other parameters are the same as in Fig. 2(b).

phase transition between $C = 0$ superfluid (SF) and $C = 2$ topological superfluid (tSF) when varying the filling. When further considering the energy spectrum of the tSF under cylinder geometry [shown in Fig. 3(a)], all the bulk modes are gapped, and two pairs of chiral edge states emerge at the two outer edges of the system [Fig. 3(b)]. It confirms that the tSF state satisfies the bulk-edge correspondence.

We now discuss the sharp distinction between our scheme for realizing higher Chern number superfluids and that proposed in previous studies [53–59]. The conventional approach relies on higher partial-wave pairing to achieve higher Chern number superfluidity. Instead, the present mechanism constructs it by engineering single-particle band structure through spin-singlet pairing by the standard s-wave attraction. The key ingredient supporting this new mechanism is that topology originates from mixing higher Wannier orbitals, rather than manipulating spins, such as in the spin-orbit coupling scheme. Typically, degenerate Wannier orbitals could emerge in the presence of point-group symmetries where the symmetry for orbitals is much lower than that for spins. Therefore, our proposal could provide an easier way of achieving higher Chern number superfluids via constructing nontrivial topology through orbital mixing. It frees up the usually challenging requirements of previous works, such as multilayer structures [53,56], spin-orbit coupling, or other artificial gauge fields [54,55,57]. This mechanism would shed light on new possibilities for edge-mode engineering through fabrication of orbital-hybridized higher Chern number phases in both electronic solids and atomic gases.

Furthermore, our scheme can significantly improve the transition temperature, making it as high as that of usual s-wave superfluidity, potentially circumventing one of the major obstacles for its realizations. It is confirmed by our study of the finite temperature phase transition. As temperature increases, the superfluid ground state undergoes the Berezinskii-Kosterlitz-Thouless (BKT) transition to the normal state [60,61]. The finite temperature phase diagram is obtained in Fig. 4 (see details in Appendix D). Since here we consider the weakly interacting regime, i.e., the interaction strength is smaller than the bandwidth, only the fermionic excitations contribute to the total normal fluid density and, thus, affect the superfluid density, whereas the contribution from collective excitations can be ignored. Therefore, the superfluid density can be calculated by using Landau's formula and to use KT-Nelson formula with mean-field results for obtaining the BKT transition temperature is available [62,63]. In current

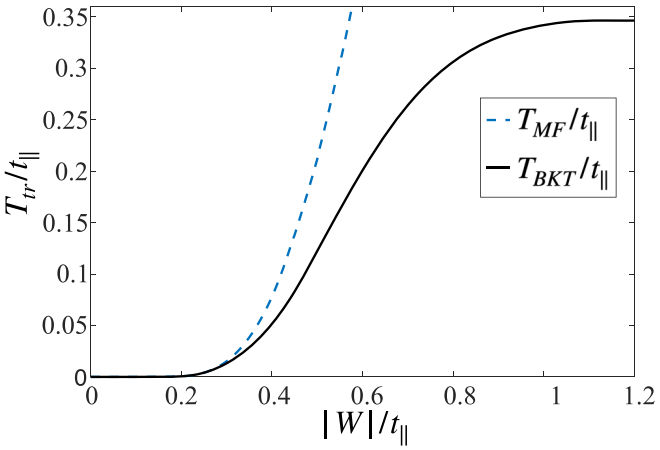

FIG. 4. Transition temperature $T_{\rm tr}$ as a function of interaction strength. Mean-field ($T_{\rm MF}$) and BKT ($T_{\rm BKT}$) transition temperature are plotted. Other parameters are the same as in Fig. 3.

experiments, such as with ^{40}K [64–66], taking advantage of the Feshbach resonance technique, the atomic interactions are highly tunable. The BKT transition temperature can reach around 19 nK, being within the experimental temperature scope. We would also like to stress that, although on-site rotation is considered in our scheme, heating from it can be suppressed in a controlled way. To evaluate the heating rate that arises from the interaction of atoms with the light, we calculate the photon-scattering rate [67,68] by employing the method in Ref. [67], which is directly related to the heating power. After somewhat tedious calculation (see details in Appendix B), the maximal heating rate can be determined by the scattering rate $\bar{\Gamma}_{\rm SC}$ through the following relation:

$$\dot{T}_{\rm heat} = \frac{E_R \bar{\Gamma}_{\rm SC}}{3k_B}, \tag{8}$$

with E_R being the recoil energy. For instance, when considering $V_x = V_y \equiv V$, $V/E_R = 5$, $V_z/V = 5$ and $a_{x(y)} = 850$ nm, the maximum heating rate for ^{40}K system is evaluated to be around 10 nK/s. Therefore, our proposed higher Chern number superfluids should have the order of a second in lifetime even in the presence of on-site rotation, making it suitable for the experimental measurement. It should potentially circumvent one of the major challenges of the heating problem, such as in the Raman-induced spin-orbit coupling scheme in ultracold gases [8].

IV. CONCLUSIONS

We have demonstrated a symmetry-based method of engineering nontrivial orbital hybridization in optical lattices. Various orbital-hybridized topological phenomena, including transformation of orbital-hybridized topological defects in single-particle bands as well as orbital-hybridized higher Chern number superfluid, have been predicted. Moreover, the mechanism can be easily achieved in current experiments by utilizing our protocol of manipulating inversion symmetry in optical lattices, potentially circumventing the challenges of the Raman-induced spin-orbit coupling scheme. The present approach, thus, complements with a new window to investigate orbital-hybridized topological phases in ultracold gases.

ACKNOWLEDGMENTS

This work was supported by the National Key R&D Program of China (Grant No. 2021YFA1401700), NSFC (Grants No. 12074305, No. 12147137, and No. 11774282), the National Key Research and Development Program of China (Grant No. 2018YFA0307600) and Xiaomi Young Scholar Program (M.A., S.L., S.H., and B.L.), and by the AFOSR Grant No. FA9550-16-1-0006, the MURI-ARO Grant No. W911NF17-1-0323 through UC Santa Barbara, and the Shanghai Municipal Science and Technology Major Project through the Shanghai Research Center for Quantum Sciences (Grant No. 2019SHZDZX01) (W.V.L.). We also thank the HPC platform of Xi'An Jiaotong University where our numerical calculations were performed.

APPENDIX A: LOW-ENERGY EFFECTIVE HAMILTONIAN AROUND TOPOLOGICAL BAND TOUCHING POINTS

In this Appendix, we provide a detailed derivation of the effective Hamiltonian in the vicinity of band touching points. The method of Feshbach projectors [69] is used to reduce the model in Eq. (2) to an effective low-energy Hamiltonian, valid around band touching points. Projection operators $\mathbf{P}$ and $\mathbf{Q} = 1 - \mathbf{P}$ are introduced, which project into the subspaces spanned by the two touching bands and the remaining band, respectively. The eigenvalue problem associated with the model Hamiltonian $\mathbf{H_0}$ can be written as $\mathbf{H_0}|\Psi\rangle = E|\Psi\rangle$, where $|\Psi\rangle$ is the eigenstate with energy E. The effective Hamiltonian $\mathbf{H}_{\rm eff}$ which describes low-energy physics near the

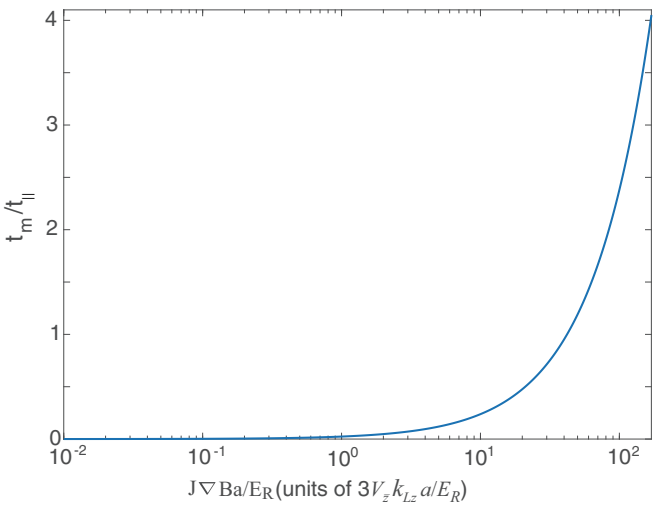

FIG. 5. The orbital hybridization $t_m/t_{\|}$ as a function of either the magnetic field gradient, or the depth $V_{\tilde{z}}$ of the additional z-directional standing wave pattern. Here, we consider the case with $\delta\mu_x = 0$ and choose $V \equiv V_x = V_y$, $\theta = \pi/2$ in the potential $V_{\tilde{z}}\cos^2(3k_{Lz}z + \theta/2)$, where E_R is the recoil energy defined as $E_R = \frac{\hbar^2 k_L^2}{2m}$ with $a \equiv a_x = a_y$ and $k_L = \pi/a$.

band touching can be obtained from

$$\left(\mathbf{PH_0P}+\mathbf{PH_0Q}\frac{1}{E-\mathbf{QH_0Q}}\mathbf{QH_0P}\right)\mathbf{P}|\Psi\rangle\equiv\mathbf{H}_{\rm eff}\mathbf{P}|\Psi\rangle=E\mathbf{P}|\Psi\rangle. \tag{A1}$$

By computing relevant matrix elements in Eq. (A1), the effective Hamiltonian $\mathbf{H}_{\rm eff}$ can be further expressed as

$$\mathbf{H}_{\rm eff}=\begin{pmatrix}2t_\parallel\cos(k_xa_x)-2t_\perp\cos(k_ya_y)-\delta\mu_x & 0\\ 0 & 2t'_\parallel\cos(k_ya_y)-2t'_\perp\cos(k_xa_x)\end{pmatrix}+\frac{2}{\bar{t}_\parallel-\bar{t}_\perp+t_z\cos(k_xa_x)+t'_z\cos(k_ya_y)}$$
$$\times\begin{pmatrix}t_m^2\sin^2(k_xa_x) & t_mt'_m\sin(k_xa_x)\sin(k_ya_y)\\ t_mt'_m\sin(k_xa_x)\sin(k_ya_y) & t'^2_m\sin^2(k_ya_y)\end{pmatrix}, \tag{A2}$$

where $\bar{t}_\parallel=(t_\parallel+t'_\parallel)/2$, $\bar{t}_\perp=(t_\perp+t'_\perp)/2$. When $\delta\mu_x\neq0$, the effective Hamiltonian near one of the Dirac touching points, for instance $(k_{\rm Dirac},0)$, can be obtained through expanding Eq. (A2) to the leading order in momentum near that Dirac point. Therefore, $\mathbf{H}_{\rm eff}^{\rm Dirac}$ can be further approximated as

$$\mathbf{H}_{\rm eff}^{\rm Dirac}\approx c'_0k'_x\mathbb{I}_{2\times2}+c'_1k_y\sigma_x+c'_3k'_x\sigma_z, \tag{A3}$$

where $k'_x=k_x-k_{\rm Dirac}$, $c'_0=-a_x(t_\parallel-t'_\perp)\sin(k_{\rm Dirac}a_x)+\frac{2a_xt_m^2\sin(k_{\rm Dirac}a_x)\cos(k_{\rm Dirac}a_x)}{\bar{t}_\parallel-\bar{t}_\perp+t'_z+t_z\cos(k_{\rm Dirac}a_x)}+\frac{2a_xt_zt_m^2\sin^3(k_{\rm Dirac}a_x)}{[\bar{t}_\parallel-\bar{t}_\perp+t'_z+t_z\cos(k_{\rm Dirac}a_x)]^2}$, $c'_1=\frac{2a_yt_mt'_m\sin(k_{\rm Dirac}a_x)}{\bar{t}_\parallel-\bar{t}_\perp+t'_z+t_z\cos(k_{\rm Dirac}a_x)}$, and $c'_3=-a_x(t_\parallel+t'_\perp)\sin(k_{\rm Dirac}a_x)+\frac{2a_xt_m^2\sin(k_{\rm Dirac}a_x)\cos(k_{\rm Dirac}a_x)}{\bar{t}_\parallel-\bar{t}_\perp+t'_z+t_z\cos(k_{\rm Dirac}a_x)}+\frac{2a_xt_zt_m^2\sin^3(k_{\rm Dirac}a_x)}{[\bar{t}_\parallel-\bar{t}_\perp+t'_z+t_z\cos(k_{\rm Dirac}a_x)]^2}$. σ_x and σ_z are the Pauli matrices and $\mathbb{I}_{2\times2}$ is the unit matrix. Eq. (A3) can also be parametrized by a vector on the (k_x,k_y) plane as

$$\mathbf{h}^{\rm Dirac}(\mathbf{k})=(c'_3k'_x,c'_1k_y). \tag{A4}$$

As shown in Fig. 1(b), the vector $\mathbf{h}^{\rm Dirac}$ defined here has a vortex structure around the Dirac points, with the winding numbers $W=\oint_C\frac{d\mathbf{k}}{2\pi}[\frac{h_x}{|\mathbf{h}|}\nabla(\frac{h_y}{|\mathbf{h}|})-\frac{h_y}{|\mathbf{h}|}\nabla(\frac{h_x}{|\mathbf{h}|})]$ being 1. Similar analysis can be performed for the case with $\delta\mu=0$. Through expanding Eq. (A2) around the Γ point in momentum space, the effective low-energy Hamiltonian around the quadratic band touching can be approximated as

$$\mathbf{H}_{\rm eff}^{\rm quadratic}\approx c_0\left(k_x^2+k_y^2\right)\mathbb{I}_{2\times2}+c_1k_xk_y\sigma_x+c_3\left(k_x^2-k_y^2\right)\sigma_z, \tag{A5}$$

where $c_0=\frac{a^2}{2}(-t_\parallel+t_\perp+\frac{2t_m^2}{t_\parallel-t_\perp+2t_z})$, $c_1=\frac{2t_m^2a^2}{t_\parallel-t_\perp+2t_z}$, and $c_3=\frac{a^2}{2}(-t_\parallel-t_\perp+\frac{2t_m^2}{t_\parallel-t_\perp+2t_z})$ with $a\equiv a_x=a_y$ and $t_\parallel/t'_\parallel=t_\perp/t'_\perp=t_m/t'_m=t_z/t'_z=1$. We further parametrize Eq. (A5) by a vector on the (k_x,k_y) plane as

$$\mathbf{h}^{\rm quadratic}(\mathbf{k})=\left[c_3\left(k_x^2-k_y^2\right),c_1k_xk_y\right]. \tag{A6}$$

The vector $\mathbf{h}^{\rm quadratic}$ also forms a vortex structure [shown in Fig. 1(d) of the main text] but with winding number W being equal to 2.

APPENDIX B: HEATING EFFECT FROM ON-SITE ROTATION

In this Appendix we make a detailed study of heating effects due to the on-site rotation term, achieved by passing laser beams forming the lattice through electro-optic phase modulators [50,51]. Let us take the case of $\delta\mu_x=0$ as example. Then, the lattice potential with electro-optic modulators can be expressed as

$$V(x,y,z)=-\frac{V}{2}\{\cos^2[k_Lx+\phi_x(t)]+\cos^2[k_Ly+\phi_y(t)]\}$$
$$-\frac{V}{4}\{\cos^2[k_Lx+k_Ly+\phi_+(t)]+\cos^2[k_Lx-k_Ly+\phi_-(t)]\}-V_z\cos^2(k_{L_z}z), \tag{B1}$$

where $V\equiv V_x=V_y$, $k_L\equiv k_{L_x}=k_{L_y}$ and the electro-optic phase modulations $\phi_x(t)=\Delta\phi\cos(\Omega_zt)\cos(\omega_{\rm RF}t)$, $\phi_y(t)=\Delta\phi\cos(\Omega_zt+\pi/2)\cos(\omega_{\rm RF}t)$, $\phi_+(t)=\Delta\phi\cos(\Omega_zt+\pi/4)\cos(\omega_{\rm RF}t)$, $\phi_-(t)=\Delta\phi\cos(\Omega_zt-\pi/4)\cos(\omega_{\rm RF}t)$ with the amplitude of oscillations $\Delta\phi$, slow precession frequency Ω_z, and the fast rotation frequency $\omega_{\rm RF}$ at radio frequency. It results in a periodical overall translation of the lattice at a radio-frequency $\omega_{\rm RF}$. The atoms do not follow fast oscillations with radio frequency $\omega_{\rm RF}$ and only feel a time-averaged potential. Local potential near each site minimum in the frame rotating with angular frequency Ω_z can be approximately (and dropping a constant) expressed as

$$V(x',y',z)\approx-\frac{3V}{2}\left(1-\frac{\Delta\phi^2}{4}\right)+\frac{m\omega'^2r'^2}{2}[1+2\epsilon\cos(2\phi')]+V_zk_{L_z}^2z^2, \tag{B2}$$

where $\frac{m\omega'^2}{2} = Vk_L^2(1-\frac{\Delta\phi^2}{2})$, $\epsilon = -\frac{\Delta\phi^2}{8(1-\Delta\phi^2/2)}$, $r'^2 = x'^2 + y'^2$ and ϕ' is the polar angle of $\mathbf{r}'$. The reference frame with rotation axis along the z direction and angular velocity Ω_z with respect to the original frame can be captured by the following transformation: $\binom{x'}{y'} = \begin{pmatrix}\cos(\Omega_z t) & -\sin(\Omega_z t)\\ \sin(\Omega_z t) & \cos(\Omega_z t)\end{pmatrix}\binom{x}{y}$. The slight deformation of the optical potential, i.e., the fourth term on the right-hand side of Eq. (B2), precesses around each site center and can be regarded as stirring the on-site rotation [50,51].

In the following, we analyze in detail the rate of heating which arises from interactions of the atom with the light. Heating power is directly related to the photon scattering rate $\Gamma_{\rm SC}$ [67,68]. To obtain that, we employ the method of Ref. [67]. The laser beams which form the lattice potential in Eq. (B1) can be expressed as

$$\begin{aligned}\mathbf{E}(x,y,z,t) &= 2\mathbf{E_x}\cos[k_L x+\phi_x(t)]\cos(\omega t) + 2\mathbf{E_y}\cos[k_L y+\phi_y(t)]\cos(\omega t) + 2\mathbf{E_z}\cos(k_{L_z} z)\cos(\omega_z t)\\ &\quad + 2\mathbf{E}_+\cos[k_L(x+y)+\phi_+(t)]\cos\left(\omega t+\frac{\pi}{2}\right) + 2\mathbf{E}_-\cos[k_L(x-y)+\phi_-(t)]\cos\left(\omega t+\frac{\pi}{2}\right),\end{aligned} \tag{B3}$$

where $\mathbf{E_x} = E\mathbf{e_z}$, $\mathbf{E_y} = E\mathbf{e_x}$, $\mathbf{E_z} = E_z\mathbf{e_y}$, $\mathbf{E}_+ = E(\mathbf{e_y}-\mathbf{e_x})/2$, and $\mathbf{E}_- = E(\mathbf{e_y}+\mathbf{e_x})/2$, with $\mathbf{e_x}$, $\mathbf{e_y}$, and $\mathbf{e_z}$ being the unit vectors along the x, y, and z directions, respectively. The dipole potential that results from the above laser fields [67] can, thus, be expressed as $U_{\rm dip} = -\frac{1}{2}\langle\mathbf{p}(x,y,z,t)\cdot\mathbf{E}(x,y,z,t)\rangle$, where $\langle\cdots\rangle$ denotes time averaging over rapid oscillations. $\mathbf{p}(x,y,z,t)$ is the dipole moment, which can be defined as $\mathbf{p}(\mathbf{r},t) = \alpha(\omega)\mathbf{E}(\mathbf{r},t)$ with the polarizability $\alpha(\omega) = \frac{e^2}{m_e}\frac{1}{\omega_0^2-\omega^2-i\omega\Gamma_\omega}$. Here, e and m_e are the charge and mass of electron, respectively, ω_0 is the frequency of the atomic transition, and $\Gamma_\omega = \omega^2\Gamma_0/\omega_0^2$ with Γ_0 being the decay rate of the electronic excited state, such as $|^2P_{1/2}\rangle$ of ^{40}K. Such a dipole potential $U_{\rm dip}$ exactly produces the lattice potential in Eq. (B1).

The rate of heating can then be evaluated by considering the atom as a classical oscillator subject to the above dipole potential. Energy absorbed by the oscillator from the driving field [67] is given by $P_{\rm abs} = \langle\dot{\mathbf{p}}(x,y,z,t)\cdot\mathbf{E}(x,y,z,t)\rangle$. Such an absorption results from the imaginary part of the polarizability, which describes the out-of-phase component of the dipole oscillation. It can be interpreted in terms of photon scattering in cycles of absorption and subsequent spontaneous reemisson processes. Such a photon scattering rate is directly related to the heating rate. Therefore, we can use $P_{\rm abs}$ to estimate the heating rate caused by the phase modulations in Eq. (B1). We next expand the electric field in $P_{\rm abs}$ in powers of small $\Delta\phi$ as $\mathbf{E}(x,y,z,t) = \mathbf{E^{(0)}}(x,y,z,t) + \mathbf{E^{(1)}}(x,y,z,t)\Delta\phi + \mathbf{E^{(2)}}(x,y,z,t)\Delta\phi^2 + \cdots$ and $P_{\rm abs}$ can, thus, be approximated as

$$P_{\rm abs} \approx P^{(0)} + \Delta\phi^2 P\cdots. \tag{B4}$$

To estimate the maximum heating rate resulting from the small phase modulations, we take the quadratic expansion term of $\Delta\phi$ in $P_{\rm abs}$ and evaluate the maximum of $P_{\rm abs}$ as $\bar{P}_{\rm abs} = \max(P^{(0)} + P^{(2)}\Delta\phi^2)$. Therefore, the maximum scattering rate $\bar{\Gamma}_{\rm SC}$ can be obtained from the following relation $\bar{\Gamma}_{\rm SC} = \bar{P}_{\rm abs}/\hbar\omega$ with $\hbar\omega = \sqrt{4VE_R}$ and the recoil energy $E_R = \hbar^2k_L^2/2m$. The maximum heating rate can, thus, be determined from the scattering rate through

$$\dot{T}_{\rm heat} = \frac{E_R\bar{\Gamma}_{\rm SC}}{3k_B}. \tag{B5}$$

To compare with realistic experimental system, for instance, we can consider the atomic transition between the $^2P_{1/2}$ and $^2S_{1/2}$ levels of ^{40}K. It is known that for this atomic transition in ^{40}K $\Gamma_0 = 2\pi\times 6$ MHz [70]. When $V/E_R = 5$, $V_z/V = 5$, $a = 2\pi/k_L = 850$ nm, and $\Delta\phi = 0.1$, the maximum heating rate is evaluated as $\dot{T}_{\rm heat} \approx 10$ nK/s. Since the estimated BKT transition temperature of our proposed higher Chern number superfluids is around 19 nk, comparing it to the heating rate obtained above, the proposed higher Chern number superfluids should have a lifetime of the order order of a second, making it suitable for experimental measurements. Therefore, our scheme should potentially circumvent the challenges of the heating problem, such as in the Raman-induced spin-orbit coupling scheme in ultracold gases.

APPENDIX C: PATH-INTEGRAL FORMALISM

By introducing Grassmann fields $\bar{C}_{\mu(\nu),\sigma}(\mathbf{r_i},\tau)$, $C_{\mu(\nu),\sigma}(\mathbf{r_i},\tau)$ with $\mu(\nu) = p_x, p_y, p_z$ and $\sigma = \uparrow,\downarrow$, which represent fermionic fields, the partition function of the system can be expressed as (the units are chosen as $\hbar = k_B = 1$)

$$\mathcal{Z} = \int \mathcal{D}\bar{C}\,\mathcal{D}C\,\exp(-S[\bar{C},C]), \tag{C1}$$

with the action S,

$$S = S_0[\bar{C},C] + S_{\rm int}[\bar{C},C], \tag{C2}$$

where

$$S_0[\bar{C},C] = \int_0^\beta d\tau \sum_{\mu\nu\mathbf{r_i}\mathbf{r}'_{\mathbf{i}}\sigma} \bar{C}_{\mu,\sigma}(\mathbf{r_i},\tau)(\delta_{\mu\nu}\delta_{\mathbf{r_i},\mathbf{r}'_{\mathbf{i}}}\partial_\tau + \mathscr{H}_{\mu\nu})C_{\nu,\sigma}(\mathbf{r}'_{\mathbf{i}},\tau),$$

$$S_{\rm int}[\bar{C}, C] = W \int_0^\beta d\tau \sum_{\mathbf{r_i}} \Bigg\{ 3 \sum_{\mu} \bar{C}_{\mu,\uparrow}(\mathbf{r_i}, \tau)\bar{C}_{\mu,\downarrow}(\mathbf{r_i}, \tau)C_{\mu,\downarrow}(\mathbf{r_i}, \tau)C_{\mu,\uparrow}(\mathbf{r_i}, \tau) + \sum_{\mu\neq\nu} \bar{C}_{\mu,\uparrow}(\mathbf{r_i}, \tau)\bar{C}_{\mu,\downarrow}(\mathbf{r_i}, \tau)C_{\nu,\downarrow}(\mathbf{r_i}, \tau)C_{\nu,\uparrow}(\mathbf{r_i}, \tau)$$
$$+ \sum_{\mu\neq\nu} \bar{C}_{\mu,\uparrow}(\mathbf{r_i}, \tau)\bar{C}_{\nu,\downarrow}(\mathbf{r_i}, \tau)C_{\mu,\downarrow}(\mathbf{r_i}, \tau)C_{\nu,\uparrow}(\mathbf{r_i}, \tau) + \sum_{\mu\neq\nu} \bar{C}_{\mu,\uparrow}(\mathbf{r_i}, \tau)\bar{C}_{\nu,\downarrow}(\mathbf{r_i}, \tau)C_{\nu,\downarrow}(\mathbf{r_i}, \tau)C_{\mu,\uparrow}(\mathbf{r_i}, \tau) \Bigg\}, \tag{C3}$$

where $U = 3W$ is assumed. The quartic fermionic interaction term in the action S can be decoupled by introducing Hubbard-Stratonovich fields

$$\bar{\Delta}^{(j)}_{\mu\nu}(\mathbf{r_i}, \tau) \quad \text{and} \quad \Delta^{(j)}_{\mu\nu}(\mathbf{r_i}, \tau), \quad \text{where } j = \begin{cases} 1, & \mu = \nu, \\ 1, 2, & \mu \neq \nu, \end{cases} \quad \text{and} \quad \mu, \nu = p_x, p_y, p_z. \tag{C4}$$

Then, the interaction part of the partition function can be rewritten as follows:

$$\int \mathcal{D}\bar{C}\,\mathcal{D}C \exp\Bigg(-W \int_0^\beta d\tau \sum_{\mathbf{r_i}} \Bigg\{ 3 \sum_{\mu} \bar{C}_{\mu,\uparrow}(\mathbf{r_i}, \tau)\bar{C}_{\mu,\downarrow}(\mathbf{r_i}, \tau)C_{\mu,\downarrow}(\mathbf{r_i}, \tau)C_{\mu,\uparrow}(\mathbf{r_i}, \tau)$$
$$+ \sum_{\mu\neq\nu} \bar{C}_{\mu,\uparrow}(\mathbf{r_i}, \tau)\bar{C}_{\mu,\downarrow}(\mathbf{r_i}, \tau)C_{\nu,\downarrow}(\mathbf{r_i}, \tau)C_{\nu,\uparrow}(\mathbf{r_i}, \tau) \Bigg\} \Bigg)$$
$$= \int \mathcal{D}\bar{C}\,\mathcal{D}C \prod_{\mu} \mathcal{D}\bar{\Delta}^{(1)}_{\mu\mu}\mathcal{D}\Delta^{(1)}_{\mu\mu} \int \exp\Bigg(\int_0^\beta d\tau \sum_{\mathbf{r_i}} \sum_{\mu\neq\nu} \Bigg\{ \frac{3\bar{\Delta}^{(1)}_{\mu\mu}(\mathbf{r_i}, \tau)\Delta^{(1)}_{\mu\mu}(\mathbf{r_i}, \tau)}{W} + \frac{\bar{\Delta}^{(1)}_{\mu\mu}(\mathbf{r_i}, \tau)\Delta^{(1)}_{\nu\nu}(\mathbf{r_i}, \tau)}{W} \Bigg\}$$
$$+ \int_0^\beta d\tau \sum_{\mathbf{r_i}} \sum_{\mu\neq\nu} \Big\{ \big[3\bar{\Delta}^{(1)}_{\mu\mu}(\mathbf{r_i}, \tau) + \bar{\Delta}^{(1)}_{\nu\nu}(\mathbf{r_i}, \tau) \big] C_{\mu,\downarrow}(\mathbf{r_i}, \tau)C_{\mu,\uparrow}(\mathbf{r_i}, \tau)$$
$$+ \big[3\Delta^{(1)}_{\mu\mu}(\mathbf{r_i}, \tau) + \Delta^{(1)}_{\nu\nu}(\mathbf{r_i}, \tau) \big] \bar{C}_{\mu,\uparrow}(\mathbf{r_i}, \tau)\bar{C}_{\mu,\downarrow}(\mathbf{r_i}, \tau) \Big\} \Bigg), \tag{C5}$$

In the cases of $\mu, \nu = p_y, p_z$ and $\mu, \nu = p_x, p_z$, the corresponding expressions can be derived in the same way. We next introduce the following Fourier transformations,

$$C_{\mu,\mathbf{k},n,\sigma} = \frac{1}{\sqrt{\beta N}} \int_0^\beta \sum_{\mathbf{r}} C_{\mu,\sigma}(\mathbf{r}, \tau) e^{i\omega_n\tau - i\mathbf{k}\cdot\mathbf{r}}\, d\tau, \qquad \bar{C}_{\mu,\mathbf{k},n,\sigma} = \frac{1}{\sqrt{\beta N}} \int_0^\beta \sum_{\mathbf{r}} \bar{C}_{\mu,\sigma}(\mathbf{r}, \tau) e^{-i\omega_n\tau + i\mathbf{k}\cdot\mathbf{r}}\, d\tau,$$
$$\Delta^{(j)}_{\mu\nu,\mathbf{q},m} = \frac{1}{\sqrt{\beta N}} \int_0^\beta \sum_{\mathbf{r}} \Delta^{(j)}_{\mu\nu}(\mathbf{r}, \tau) e^{i\varpi_m\tau - i\mathbf{q}\cdot\mathbf{r}}\, d\tau, \qquad \bar{\Delta}^{(j)}_{\mu\nu,\mathbf{q},m} = \frac{1}{\sqrt{\beta N}} \int_0^\beta \sum_{\mathbf{r}} \bar{\Delta}^{(j)}_{\mu\nu}(\mathbf{r}, \tau) e^{-i\varpi_m\tau + i\mathbf{q}\cdot\mathbf{r}}\, d\tau, \tag{C6}$$

where N is the total number of lattice sites and $\omega_n = (2n+1)n/\beta$, $\varpi_m = 2m\pi/\beta$ with $\beta = 1/T$ are the fermionic and bosonic Matsubara frequencies, respectively. Since the superfluid state investigated here is the BCS-type, we can further approximately rewrite the Hubbard-Stratonovich fields representing the fermionic pairing as

$$\Delta^{(j)}_{\mu\nu,\mathbf{q},m} = \sqrt{\beta N}\delta_{\mathbf{q},0}\delta_{m,0}\Delta^{(j)}_{\mu\nu},$$
$$\bar{\Delta}^{(j)}_{\mu\nu,\mathbf{q},m} = \sqrt{\beta N}\delta_{\mathbf{q},0}\delta_{m,0}\bar{\Delta}^{(j)}_{\mu\nu}. \tag{C7}$$

Then the partition function becomes

$$\mathcal{Z} = \int \mathcal{D}\{\bar{C}, C, \bar{\Delta}^{(j)}, \Delta^{(j)}\} \exp(-S_{\rm sp}[\bar{C}, C, \bar{\Delta}^{(j)}, \Delta^{(j)}]),$$

$$\begin{aligned} S_{\rm sp}[\bar{C}, C, \bar{\Delta}, \Delta] = &- \frac{N\beta}{W}\sum_{\mu\neq\nu}\left(3\bar{\Delta}^{(1)}_{\mu\mu}\Delta^{(1)}_{\mu\mu} + \bar{\Delta}^{(1)}_{\mu\mu}\Delta^{(1)}_{\nu\nu}\right) - \frac{N\beta}{W}\sum_{\substack{\mu\nu=\{p_xp_y,\\ p_yp_z,p_zp_x\}}}\left(\bar{\Delta}^{(1)}_{\mu\nu}\Delta^{(2)}_{\mu\nu} + \bar{\Delta}^{(2)}_{\nu\mu}\Delta^{(1)}_{\nu\mu} + \bar{\Delta}^{(1)}_{\nu\mu}\Delta^{(1)}_{\mu\nu} + \bar{\Delta}^{(2)}_{\mu\nu}\Delta^{(2)}_{\nu\mu}\right) \\ &+ \sum_{\mathbf{k},n,\mu,\nu,\sigma}\bar{C}_{\mu,\mathbf{k},n,\sigma}(-i\omega_n\delta_{\mu\nu} + [\mathscr{H}(\mathbf{k})]_{\mu\nu})C_{\nu,\mathbf{k},n,\sigma} - \sum_{\substack{\mathbf{k},n\\ \mu\neq\nu}}\Big(\left[3\bar{\Delta}^{(1)}_{\mu\mu} + \bar{\Delta}^{(1)}_{\nu\nu}\right]C_{\mu,-\mathbf{k},-n,\downarrow}C_{\mu,\mathbf{k},n,\uparrow} \\ &+ \left[3\Delta^{(1)}_{\mu\mu} + \Delta^{(1)}_{\nu\nu}\right]\bar{C}_{\mu,\mathbf{k},n,\uparrow}\bar{C}_{\mu,-\mathbf{k},-n,\downarrow}\Big) - \sum_{\substack{\mathbf{k},n\\ \mu\nu=\{p_xp_y,\\ p_yp_z,p_zp_x\}}}\Big(\left[\bar{\Delta}^{(1)}_{\mu\nu} + \bar{\Delta}^{(1)}_{\nu\mu}\right]C_{\mu,-\mathbf{k},-n,\downarrow}C_{\nu,\mathbf{k},n,\uparrow} \\ &+ \left[\Delta^{(1)}_{\mu\nu} + \Delta^{(1)}_{\nu\mu}\right]\bar{C}_{\mu,\mathbf{k},n,\uparrow}\bar{C}_{\nu,-\mathbf{k},-n,\downarrow}\Big) - \sum_{\substack{\mathbf{k},n\\ \mu\nu=\{p_yp_x,\\ p_zp_y,p_xp_z\}}}\left(\left[\bar{\Delta}^{(2)}_{\mu\nu} + \bar{\Delta}^{(2)}_{\nu\mu}\right]C_{\mu,-\mathbf{k},-n,\downarrow}C_{\nu,\mathbf{k},n,\uparrow}\right. \\ &\left.+ \left[\Delta^{(2)}_{\mu\nu} + \Delta^{(2)}_{\nu\mu}\right]\bar{C}_{\mu,\mathbf{k},n,\uparrow}\bar{C}_{\nu,-\mathbf{k},-n,\downarrow}\right). \end{aligned}$$

We, then, further rewrite the action in the Nambu representation,

$$\begin{aligned} S_{\rm sp}[\bar{C}, C, \bar{\Delta}, \Delta] = &- \frac{N\beta}{W}\sum_{\mu\neq\nu}\left(3\bar{\Delta}^{(1)}_{\mu\mu}\Delta^{(1)}_{\mu\mu} + \bar{\Delta}^{(1)}_{\mu\mu}\Delta^{(1)}_{\nu\nu}\right) - \frac{N\beta}{W}\sum_{\substack{\mu\nu=\{p_xp_y,\\ p_yp_z,p_zp_x\}}}\left(\bar{\Delta}^{(1)}_{\mu\nu}\Delta^{(2)}_{\mu\nu} + \bar{\Delta}^{(2)}_{\nu\mu}\Delta^{(1)}_{\nu\mu} + \bar{\Delta}^{(1)}_{\nu\mu}\Delta^{(1)}_{\mu\nu} + \bar{\Delta}^{(2)}_{\mu\nu}\Delta^{(2)}_{\nu\mu}\right) \\ &+ \sum_{\mathbf{k},n}\bar{\eta}_{\mathbf{k},n}[-i\omega_n\mathbb{I}_6 + H_{\rm BdG}(\mathbf{k})]\eta_{\mathbf{k},n}, \end{aligned}$$

where $\eta_{\mathbf{k},n} = (C_{p_x,\mathbf{k},n,\uparrow} \quad C_{p_y,\mathbf{k},n,\uparrow} \quad C_{p_z,\mathbf{k},n,\uparrow} \quad \bar{C}_{p_x,-\mathbf{k},-n,\downarrow} \quad \bar{C}_{p_y,-\mathbf{k},-n,\downarrow} \quad \bar{C}_{p_z,-\mathbf{k},-n,\downarrow})^T$ is the Nambu spinor. $\mathbb{I}_6$ is the 6×6 unit matrix and $H_{\rm BdG}(\mathbf{k})$ is the 6×6 Bogoliubov–de Gennes matrix,

$$H_{\rm BdG}(\mathbf{k}) = \begin{pmatrix} \mathscr{H}(\mathbf{k}) & -M \\ -\overline{M} & -\mathscr{H}^T(-\mathbf{k}) \end{pmatrix},$$

with

$$M = \begin{pmatrix} 3\Delta^{(1)}_{p_xp_x} + \Delta^{(1)}_{p_yp_y} + \Delta^{(1)}_{p_zp_z} & \Delta^{(1)}_{p_xp_y} + \Delta^{(1)}_{p_yp_x} & \Delta^{(2)}_{p_xp_z} + \Delta^{(2)}_{p_zp_x} \\ \Delta^{(2)}_{p_xp_y} + \Delta^{(2)}_{p_yp_x} & 3\Delta^{(1)}_{p_yp_y} + \Delta^{(1)}_{p_xp_x} + \Delta^{(1)}_{p_zp_z} & \Delta^{(1)}_{p_yp_z} + \Delta^{(1)}_{p_zp_y} \\ \Delta^{(1)}_{p_xp_z} + \Delta^{(1)}_{p_zp_x} & \Delta^{(2)}_{p_yp_z} + \Delta^{(2)}_{p_zp_y} & 3\Delta^{(1)}_{p_zp_z} + \Delta^{(1)}_{p_xp_x} + \Delta^{(1)}_{p_yp_y} \end{pmatrix},$$

$$\overline{M} = \begin{pmatrix} 3\bar{\Delta}^{(1)}_{p_xp_x} + \bar{\Delta}^{(1)}_{p_yp_y} + \bar{\Delta}^{(1)}_{p_zp_z} & \bar{\Delta}^{(1)}_{p_xp_y} + \bar{\Delta}^{(1)}_{p_yp_x} & \bar{\Delta}^{(2)}_{p_xp_z} + \bar{\Delta}^{(2)}_{p_zp_x} \\ \bar{\Delta}^{(2)}_{p_xp_y} + \bar{\Delta}^{(2)}_{p_yp_x} & 3\bar{\Delta}^{(1)}_{p_yp_y} + \bar{\Delta}^{(1)}_{p_xp_x} + \bar{\Delta}^{(1)}_{p_zp_z} & \bar{\Delta}^{(1)}_{p_yp_z} + \bar{\Delta}^{(1)}_{p_zp_y} \\ \bar{\Delta}^{(1)}_{p_xp_z} + \bar{\Delta}^{(1)}_{p_zp_x} & \bar{\Delta}^{(2)}_{p_yp_z} + \bar{\Delta}^{(2)}_{p_zp_y} & 3\bar{\Delta}^{(1)}_{p_zp_z} + \bar{\Delta}^{(1)}_{p_xp_x} + \bar{\Delta}^{(1)}_{p_zp_z} \end{pmatrix}. \tag{C8}$$

Integrating out the fermionic fields, the partition function can be expressed as

$$\mathcal{Z} = \exp[-\beta N F_{\rm sp}(\bar{\Delta}, \Delta, T, \mu)], \tag{C9}$$

$$\begin{aligned} F_{\rm sp}(\bar{\Delta}, \Delta, T, \mu) = &- \frac{1}{W}\sum_{\mu\neq\nu}\left(3\bar{\Delta}^{(1)}_{\mu\mu}\Delta^{(1)}_{\mu\mu} + \bar{\Delta}^{(1)}_{\mu\mu}\Delta^{(1)}_{\nu\nu}\right) - \frac{1}{W}\sum_{\substack{\mu\nu=\{p_xp_y,\\ p_yp_z,p_zp_x\}}}\left(\bar{\Delta}^{(1)}_{\mu\nu}\Delta^{(2)}_{\mu\nu} + \bar{\Delta}^{(2)}_{\nu\mu}\Delta^{(1)}_{\nu\mu} + \bar{\Delta}^{(1)}_{\nu\mu}\Delta^{(1)}_{\mu\nu} + \bar{\Delta}^{(2)}_{\mu\nu}\Delta^{(2)}_{\nu\mu}\right) \\ &- \frac{1}{N\beta}\sum_{\mathbf{k},n}\ln\{-\det[-i\omega_n\mathbb{I}_6 + H_{\rm BdG}(\mathbf{k})]\}. \end{aligned}$$

Then, the average filling of the system and the saddle-point values of the Hubbard-Stratonovich fields representing fermionic pairing can be determined from

$$n = -\frac{\partial F_{\rm sp}(\bar{\Delta}, \Delta, T, \mu)}{\partial \mu}, \qquad \frac{\partial F_{\rm sp}(\bar{\Delta}, \Delta, T, \mu)}{\partial \bar{\Delta}^{(j)}_{\mu\nu}} = 0, \qquad \frac{\partial F_{\rm sp}(\bar{\Delta}, \Delta, T, \mu)}{\partial \Delta^{(j)}_{\mu\nu}} = 0. \tag{C10}$$

From Eq. (C10), we can define the pairing order parameters as $\Delta_{\mu\nu} \equiv \Delta^{(1)}_{\mu\nu}$, $\Delta^*_{\mu\nu} \equiv \bar{\Delta}^{(1)}_{\mu\nu}$ when $\mu = \nu$, and for $\mu \neq \nu$, $\Delta_{\mu\nu} \equiv \Delta^{(1)}_{\mu\nu} = \Delta^{(2)}_{\mu\nu}$, $\Delta^*_{\mu\nu} \equiv \bar{\Delta}^{(1)}_{\mu\nu} = \bar{\Delta}^{(2)}_{\mu\nu}$. Therefore, we can rewrite the $H_{\rm BdG}(\mathbf{k})$ as

$$H_{\rm BdG}(\mathbf{k}) = \begin{pmatrix} \mathscr{H}(\mathbf{k}) & -M \\ -(M^T)^* & -\mathscr{H}^T(-\mathbf{k}) \end{pmatrix},$$

$$M = \begin{pmatrix} 3\Delta_{p_xp_x} + \Delta_{p_yp_y} + \Delta_{p_zp_z} & \Delta_{p_xp_y} + \Delta_{p_yp_x} & \Delta_{p_xp_z} + \Delta_{p_zp_x} \\ \Delta_{p_xp_y} + \Delta_{p_yp_x} & 3\Delta_{p_yp_y} + \Delta_{p_xp_x} + \Delta_{p_zp_z} & \Delta_{p_yp_z} + \Delta_{p_zp_y} \\ \Delta_{p_xp_z} + \Delta_{p_zp_x} & \Delta_{p_yp_z} + \Delta_{p_zp_y} & 3\Delta_{p_zp_z} + \Delta_{p_xp_x} + \Delta_{p_yp_y} \end{pmatrix}. \tag{C11}$$

APPENDIX D: BEREZINSKII-KOSTERLITZ-THOULESS TRANSITION

It is well known that at finite temperature superfluidity of 2D atomic Fermi gases is characterized by the vortex-antivortex binding. The relevant mechanism is the Berezinskii-Kosterlitz-Thouless (BKT) phase transition occurring at a characteristic temperature $T_{\rm BKT}$ [60,61]. The BKT transition in 2D is associated with spontaneous formation of vortices. A unique feature of such a transition is a universal jump in the superfluid density, also known as the Nelson-Kosterlitz jump [71]. To further determine the superfluid density, we impose a phase twist (e.g., see Refs. [72–74]) (i.e., supercurrent) on the order parameter as

$$\Delta_{\mu\nu} \to \Delta_{\mu\nu} \exp\left(i \cdot 2\boldsymbol{\Theta} \cdot \mathbf{r_i}\right) = \Delta_{\mu\nu} \exp\left(i\frac{2\Theta_x n_x}{N_x} + i\frac{2\Theta_y n_y}{N_y}\right), \tag{D1}$$

where $\mathbf{r_i} = n_x a_x \vec{e}_x + n_y a_y \vec{e}_y$ label the lattice sites. $\boldsymbol{\Theta}$ captures linear phase variation on the order parameter and N_x and N_y represent the numbers of sites along the x and y directions, respectively. The imposed phase gradient introduces extra kinetic energy into the system, which corresponds to the difference of free energies $\Delta F \equiv F_{\boldsymbol{\Theta}} - F_0$, where $F_{\boldsymbol{\Theta}}$ and F_0 are the free energies within and without the phase variation, respectively. We then approximate ΔF up to the second order in $\boldsymbol{\Theta}$ as $\Delta F \simeq \sum_{\alpha,\beta=x,y} F^{(2)}_{\alpha\beta}\Theta_\alpha\Theta_\beta$. Due to the reflection symmetry of the system, when $\alpha \neq \beta$, $F^{(2)}_{\alpha\beta}$ vanishes, and we further have

$$\begin{aligned} F^{(2)}_{\alpha\alpha} =& \frac{T}{2N}\sum_{\mathbf{k},n,\mu,\nu}\left[\frac{\partial^2\mathscr{H}(\mathbf{k})}{\partial^2 k_\alpha}\right]_{\mu\nu}(-[G_{\mathbf{k},n,\uparrow}]_{\nu\mu} - [G_{-\mathbf{k},-n,\downarrow}]_{\mu\nu}) + \frac{T}{2}\sum_{\mathbf{k},n,\mu,\nu,\mu',\nu'}\left[\frac{\partial\mathscr{H}(\mathbf{k})}{\partial k_\alpha}\right]_{\mu\nu}\left[\frac{\partial\mathscr{H}(\mathbf{k})}{\partial k_\alpha}\right]_{\mu'\nu'} \\ &\times([G_{\mathbf{k},n,\uparrow}]_{\nu\mu'}[G_{\mathbf{k},n,\uparrow}]_{\nu'\mu} + [G_{\mathbf{k},n,\downarrow}]_{\nu\mu'}[G_{\mathbf{k},n,\downarrow}]_{\nu'\mu} + [F_{\mathbf{k},n}]_{\nu\mu'}[F^\dagger_{\mathbf{k},n}]_{\nu'\mu} + [F_{\mathbf{k},n}]_{\nu'\mu}[F^\dagger_{\mathbf{k},n}]_{\nu\mu'}), \end{aligned}$$

where $[G_{\mathbf{k},n,\sigma}]_{\mu\nu} = \langle C_{\mu,\mathbf{k},n,\sigma}\bar{C}_{\nu,\mathbf{k},n,\sigma}\rangle$ and $[F_{\mathbf{k},n}]_{\mu\nu} = \langle C_{\mu,\mathbf{k},n,\uparrow}C_{\nu,-\mathbf{k},-n,\downarrow}\rangle$ are the matrix elements of the normal and anomalous Greens's functions. Then the BKT transition temperature can be determined from the Nelson-Kosterlitz jump condition $k_B T_{\rm BKT} = \frac{\pi}{4}F^{(2)}$ with $F^{(2)} \equiv (F^{(2)}_{xx} + F^{(2)}_{yy})/2$.

[1] G. E. Volovik, *The Universe in a Helium Droplet* (Oxford University Press, Oxford, 2003).
[2] M. Z. Hasan and C. L. Kane, Rev. Mod. Phys. **82**, 3045 (2010).
[3] X.-L. Qi and S.-C. Zhang, Rev. Mod. Phys. **83**, 1057 (2011).
[4] T. H. Hansson, M. Hermanns, S. H. Simon, and S. F. Viefers, Rev. Mod. Phys. **89**, 025005 (2017).
[5] K. von Klitzing, Rev. Mod. Phys. **58**, 519 (1986).
[6] L. D. Landau, E. M. Lifshitz, and L. P. Pitaevskii, *Statistical Physics* (Pergamon, New York, 1978).
[7] X.-G. Wen, *Quantum Field Theory of Many-Body Systems* (Oxford University Press, Oxford, 2007).
[8] V. Galitski and I. Spielman, Nature (London) **494**, 49 (2013).
[9] J. Dalibard, F. Gerbier, G. Juzeliūnas, and P. Öhberg, Rev. Mod. Phys. **83**, 1523 (2011).
[10] M. Lewenstein, A. Sanpera, and V. Ahufinger, *Ultracold Atoms in Optical Lattices* (Oxford University Press, Oxford, 2013).
[11] Y.-J. Lin, K. Jimenez-Garcia, and I. B. Spielman, Nature (London) **471**, 83 (2011).
[12] Z. Wu, L. Zhang, W. Sun, X.-T. Xu, B.-Z. Wang, S.-C. Ji, Y. Deng, S. Chen, X.-J. Liu, and J.-W. Pan, Science **354**, 83 (2016).
[13] L. W. Cheuk, A. T. Sommer, Z. Hadzibabic, T. Yefsah, W. S. Bakr, and M. W. Zwierlein, Phys. Rev. Lett. **109**, 095302 (2012).
[14] P. Wang, Z.-Q. Yu, Z. Fu, J. Miao, L. Huang, S. Chai, H. Zhai, and J. Zhang, Phys. Rev. Lett. **109**, 095301 (2012).
[15] C. V. Parker, L.-C. Ha, and C. Chin, Nat. Phys. **9**, 769 (2013).
[16] H. Zhai, Int. J. Mod. Phys. B **26**, 1230001 (2012).
[17] G. Jotzu, M. Messer, R. Desbuquois, M. Lebrat, T. Uehlinger, D. Greif, and T. Esslinger, Nature (London) **515**, 237 (2014).
[18] L. Duca, T. Li, M. Reitter, I. Bloch, M. Schleier-Smith, and U. Schneider, Science **347**, 288 (2015).

[19] M. Aidelsburger, M. Atala, M. Lohse, J. T. Barreiro, B. Paredes, and I. Bloch, Phys. Rev. Lett. **111**, 185301 (2013).
[20] H. Miyake, G. A. Siviloglou, C. J. Kennedy, W. C. Burton, and W. Ketterle, Phys. Rev. Lett. **111**, 185302 (2013).
[21] S.-L. Zhang and Q. Zhou, Phys. Rev. A **90**, 051601(R) (2014).
[22] W. Zheng and H. Zhai, Phys. Rev. A **89**, 061603(R) (2014).
[23] S. K. Baur, M. H. Schleier-Smith, and N. R. Cooper, Phys. Rev. A **89**, 051605(R) (2014).
[24] T. Müller, S. Fölling, A. Widera, and I. Bloch, Phys. Rev. Lett. **99**, 200405 (2007).
[25] G. Wirth, M. Ölschläger, and A. Hemmerich, Nat. Phys. **7**, 147 (2011).
[26] P. Soltan-Panahi, D.-S. Lühmann, J. Struck, P. Windpassinger, and K. Sengstock, Nat. Phys. **8**, 71 (2012).
[27] T. Kock, M. Ölschläger, A. Ewerbeck, W.-M. Huang, L. Mathey, and A. Hemmerich, Phys. Rev. Lett. **114**, 115301 (2015).
[28] K. Sun, W. V. Liu, A. Hemmerich, and S. Das Sarma, Nat. Phys. **8**, 67 (2012).
[29] X. Li, E. Zhao, and W. V. Liu, Nat. Commun. **4**, 1523 (2013).
[30] B. Liu, X. Li, B. Wu, and W. V. Liu, Nat. Commun. **5**, 5064 (2014).
[31] B. Liu, P. Zhang, H. Gao, and F. Li, Phys. Rev. Lett. **121**, 015303 (2018).
[32] E. Zhao and W. V. Liu, Phys. Rev. Lett. **100**, 160403 (2008).
[33] C. Wu, Phys. Rev. Lett. **100**, 200406 (2008).
[34] C. Wu, Phys. Rev. Lett. **101**, 186807 (2008).
[35] M. Hachmann, Y. Kiefer, J. Riebesehl, R. Eichberger, and A. Hemmerich, Phys. Rev. Lett. **127**, 033201 (2021).
[36] X.-Q. Wang, G.-Q. Luo, J.-Y. Liu, W. V. Liu, A. Hemmerich, and Z.-F. Xu, Nature (London) **596**, 227 (2021).
[37] B. Liu, X. Li, and W. V. Liu, Phys. Rev. A **93**, 033643 (2016).
[38] B. Liu, X. Li, R. G. Hulet, and W. V. Liu, Phys. Rev. A **94**, 031602(R) (2016).
[39] Z. Zhang, H.-H. Hung, C. M. Ho, E. Zhao, and W. V. Liu, Phys. Rev. A **82**, 033610 (2010).
[40] Z. Cai, Y. Wang, and C. Wu, Phys. Rev. A **83**, 063621 (2011).
[41] Z. Cai, Y. Wang, and C. Wu, Phys. Rev. B **86**, 060517(R) (2012).
[42] Z. Zhou, E. Zhao, and W. V. Liu, Phys. Rev. Lett. **114**, 100406 (2015).
[43] F. Pinheiro, G. M. Bruun, J.-P. Martikainen, and J. Larson, Phys. Rev. Lett. **111**, 205302 (2013).
[44] X. Li, Z. Zhang, and W. V. Liu, Phys. Rev. Lett. **108**, 175302 (2012).
[45] K. Sun, Z. Gu, H. Katsura, and S. Das Sarma, Phys. Rev. Lett. **106**, 236803 (2011).
[46] K. Sun and E. Fradkin, Phys. Rev. B **78**, 245122 (2008).
[47] V. Oganesyan, S. A. Kivelson, and E. Fradkin, Phys. Rev. B **64**, 195109 (2001).
[48] S. A. Kivelson, I. P. Bindloss, E. Fradkin, V. Oganesyan, J. M. Tranquada, A. Kapitulnik, and C. Howald, Rev. Mod. Phys. **75**, 1201 (2003).
[49] K. Sun, H. Yao, E. Fradkin, and S. A. Kivelson, Phys. Rev. Lett. **103**, 046811 (2009).
[50] N. Gemelke, Ph.D. thesis, Stanford University, 2007.
[51] N. Gemelke, E. Sarajlic, and S. Chu, arXiv:1007.2677.
[52] A. P. Schnyder, S. Ryu, A. Furusaki, and A. W. W. Ludwig, Phys. Rev. B **78**, 195125 (2008).
[53] T. Scaffidi and S. H. Simon, Phys. Rev. Lett. **115**, 087003 (2015).
[54] J. Röntynen and T. Ojanen, Phys. Rev. Lett. **114**, 236803 (2015).
[55] J. Li, T. Neupert, Z. Wang, A. H. MacDonald, A. Yazdani, and B. A. Bernevig, Nat. Commun. **7**, 12297 (2016).
[56] B. Huang, C. F. Chan, and M. Gong, Phys. Rev. B **91**, 134512 (2015).
[57] Y. Yi-Xiang, F. Sun, and J. Ye, Phys. Rev. B **98**, 174506 (2018).
[58] T. Senthil, J. B. Marston, and M. P. A. Fisher, Phys. Rev. B **60**, 4245 (1999).
[59] O. A. Awoga, A. Bouhon, and A. M. Black-Schaffer, Phys. Rev. B **96**, 014521 (2017).
[60] V. L. Berezinskii, Zh. Eksp. Teor. Fiz. **61**, 1144 (1972) [Sov. Phys. JETP **34**, 610 (1972)].
[61] J. Kosterlitz and D. Thouless, J. Phys. C: Solid State Phys. **6**, 1181 (1973).
[62] M. Iskin and C. A. R. Sá de Melo, Phys. Rev. B **72**, 224513 (2005).
[63] J. R. Engelbrecht, M. Randeria, and C. A. R. Sá de Melo, Phys. Rev. B **55**, 15153 (1997).
[64] S. Giorgini, L. P. Pitaevskii, and S. Stringari, Rev. Mod. Phys. **80**, 1215 (2008).
[65] C. A. Regal, M. Greiner, and D. S. Jin, Phys. Rev. Lett. **92**, 040403 (2004).
[66] J. T. Stewart, J. P. Gaebler, C. A. Regal, and D. S. Jin, Phys. Rev. Lett. **97**, 220406 (2006).
[67] R. Grimm, M. Weidemuller, and Y. Ovchinnikov, Adv. At., Mol., Opt. Phys. **42**, 95 (2000).
[68] D. C. McKay and B. DeMarco, Rep. Prog. Phys. **74**, 054401 (2011).
[69] H. Feshbach, Ann. Phys. (NY) **19**, 287 (1962).
[70] S. Falke, E. Tiemann, C. Lisdat, H. Schnatz, and G. Grosche, Phys. Rev. A **74**, 032503 (2006).
[71] D. R. Nelson and J. M. Kosterlitz, Phys. Rev. Lett. **39**, 1201 (1977).
[72] T. Paananen, J. Phys. B: At., Mol. Opt. Phys. **42**, 165304 (2009).
[73] J. P. A. Devreese, J. Tempere, and C. A. R. Sá de Melo, Phys. Rev. A **92**, 043618 (2015).
[74] Y. Yanay and E. J. Mueller, arXiv:1209.2446.